# A Study on Finite Element Simulation Methods and Structural Optimisation of the Crater Bridge

Qikai Liu and Qilin Zhao* and Haojing Wang

Nanjing Tech University, Nanjing, 210000, China
*ZHAOHSQL919@163.com

**Abstract.** To assist amphibious armoured vehicles in crossing coastal breakwaters and to rapidly repair small craters in wartime to restore road access, a small-span crater bridge with a maximum span of 5 m has been proposed. To facilitate its use by amphibious armoured vehicles, the small-span crater bridge employs a folding design concept. As a box-girder emergency bridge, the initial design failed to account for the issue of front-wheel lift-off caused by its small span and triangular structure. Consequently, the design load was still based on a uniformly distributed track load, resulting in insufficient stability of the bridge deck once the vehicle was on the bridge and ultimately leading to the collapse of the entire structure. Therefore, this paper proposes the use of a corrugated sandwich structure to optimise the bridge deck, ensuring it meets the load-bearing requirements.

**Keywords:** Corrugated sandwich structure, Box-girder emergency bridge, Structural optimisation design

## 1 Introduction

China is a vast country with diverse topography; regions such as the south-west and the south-eastern coast are prone to frequent natural disasters, including earthquakes, floods, mudslides and typhoons, which have resulted in significant loss of life and economic damage [1-2]. As essential routes spanning mountains and valleys, roads and bridges are often severely damaged during natural disasters and military conflicts, posing significant challenges to troop movements and post-disaster emergency relief efforts. To restore transport links as quickly as possible following natural or man-made disasters, research into rapidly deployable emergency bridge equipment is essential [3-4].

Early emergency bridges were generally designed and manufactured using metallic materials such as high-strength steel and aluminium alloys; however, these materials made it difficult for emergency bridges to meet higher requirements in terms of span, service life and load-bearing capacity [5-6]. As emergency bridges have evolved towards larger spans and lighter weights, composite materials with their high specific strength and specific stiffness along the fibre direction [7-8] offer a natural advantage in addressing the issues faced by traditional metallic emergency bridges, namely their heavy

© The Author(s) 2026
H. Wu et al. (eds.), *Proceedings of the 2026 3rd International Conference on Civil Engineering Structures and Concrete Materials (CESCM 2026)*, Advances in Engineering Research 312,
https://doi.org/10.2991/978-94-6239-865-8_4

weight and inability to achieve greater spans or higher load-bearing capacities [9]. However, composite materials suffer from issues such as low shear strength, insufficient strength in the cross-fibre direction, and poor wear resistance; consequently, they are not typically used as the primary load-bearing members in emergency bridges [10-11]. The primary load-bearing members remain metallic. To reduce the weight of these metallic members, they are usually designed as thin-walled structures, which results in local stability failing to meet design requirements and hinders the full utilisation of the material's strength.

This paper therefore proposes the use of a corrugated sandwich structure [12] for the structural optimisation of the metal primary load-bearing members in emergency bridges, thereby ensuring a lightweight structure whilst utilising the mechanical properties of the materials and enhancing stability.

## 2 Introduction to the Structure and Finite Element Mode

### 2.1 Introduction to the Structure

The crater bridge is supported by two parallel lanes; it is constructed from high-strength 6061-T6 aluminium alloy. Each lane is 6 m long, 0.6 m wide and 0.4 m high. The structure is a plate-shell configuration with a box-type closed cross-section featuring flanges projecting at the top and bottom. The bridge deck is designed as an orthotropic plate. The structural configuration of a single lane of the crater bridge is shown in Figure 1.

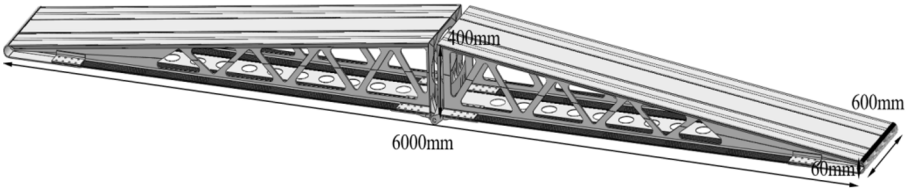



**Fig. 1.** Introduction to the Crater Bridge Structure

### 2.2 Introduction to the Finite Element Model

For box-girder emergency bridges such as the Dangkou Bridge, traditional modelling methods typically employ shell elements to simulate the various structural plates. However, as shell elements do not account for stress variations along the thickness of the element, they are unable to simulate the shear failure that occurs in the bridge deck. Consequently, solid elements are used to model the bridge deck, whilst shell elements are still employed to simulate the other structural plates in order to improve computational efficiency. The element types and material properties used for the various structural plates are shown in Figure 2, and the material properties used in the modelling are listed in Table 1.

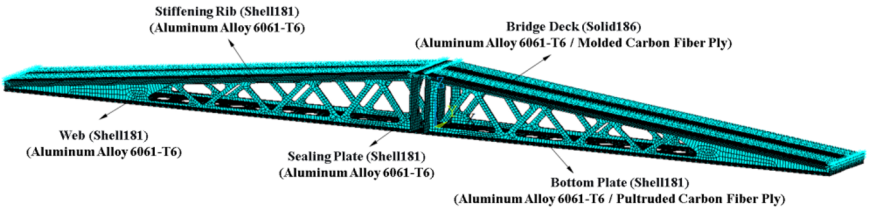



**Fig. 2.** Introduction to the finite element model

**Table 1.** Material Properties

| Material type | density/(kg/m3) | Modulus of elasticity/GPa | Poisson's ratio |
|---|---|---|---|
| Moulded carbon fibre laminate | 1900 | $E_1 = 120$<br>$E_2 = E_3 = 9$ | $v_{12} = v_{13} = v_{23} = 0.3$ |
| Pultruded carbon fibre panels | 1900 | $E_1 = 150$<br>$E_2 = E_3 = 10.2$ | $v_{12} = v_{13} = 0.26$<br>$v_{23} = 0.2$ |
| Aluminium alloy 6061-T6 | 2800 | $E = 68$ | $v = 0.33$ |

The design load is an amphibious armoured vehicle with a gross vehicle weight of 30 tonnes; each wheel track bears a load of 15 tonnes. Due to the gradient, the most critical scenario involves the vehicle's road wheels becoming airborne, at which point only two wheels are in direct contact with the bridge deck, with the front wheel bearing a load of 10.75 tonnes and the rear wheel bearing a load of 3.25 tonnes. The wheelbase between the two is 1950 mm, and the contact area between the road wheels and the bridge deck of the crater bridge is 350 mm * 100 mm. The load is applied to the bridge deck surface in the form of nodal forces, as shown in Figure 3. The finite element model is constrained with simply supported ends.

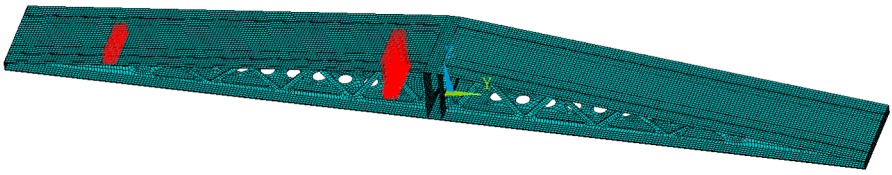


**Fig. 3.** Schematic diagram of loads

## 3 Results of the Finite Element Analysis

### 3.1 Comparison of vertical Displacement Calculation Results from the Finite Element Model

Figure 4 shows the results of the vertical displacement calculations for the finite element model. The maximum vertical displacement is 41.02 mm; at this point, the bridge

deck has already buckled and is no longer capable of bearing loads. Furthermore, the deflection of the bridge deck does not meet the design requirements, and the bridge deck must therefore be redesigned and optimised to ensure compliance with these requirements.

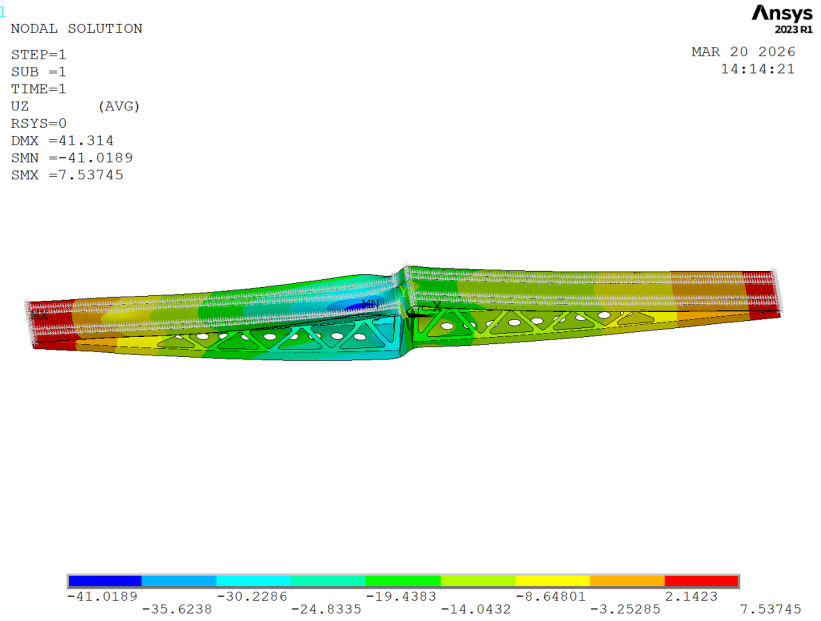



**Fig. 4.** Vertical displacement

### 3.2 Results of the Finite Element Stress Analysis

Aluminium alloy 6061-T6 has a design allowable strength of 200 MPa and a ultimate shear strength of 125 MPa. When a load is applied to the bridge deck, the structure experiences significant longitudinal stresses under bending moments; simultaneously, during full-load testing, shear failure occurred in the longitudinal section of the bridge deck at the point of load application. Therefore, the calculation results for the longitudinal stresses in the main structure are compared with those for the shear stresses in the bridge deck. Figure 5(a) shows the calculated longitudinal stresses in the bridge deck, with a maximum compressive stress of 480.33 MPa and a maximum tensile stress of 230.27 MPa. Figure 5(b) shows the calculated longitudinal stresses in the web, with maximum tensile and compressive stresses of 157.51 MPa and 157.05 MPa, respectively. Figure 5(c) shows the calculated longitudinal stresses in the bottom plate, with maximum tensile and compressive stresses of 213.43 MPa and 78.48 MPa respectively. Figure 5(d) shows the calculated shear stresses in the bridge deck, with a maximum shear stress of 133.78 MPa. The longitudinal stresses in the bridge deck far exceed the design allowable strength, and the shear stresses far exceed the ultimate shear strength; therefore, the bridge deck requires re-optimisation and redesign.

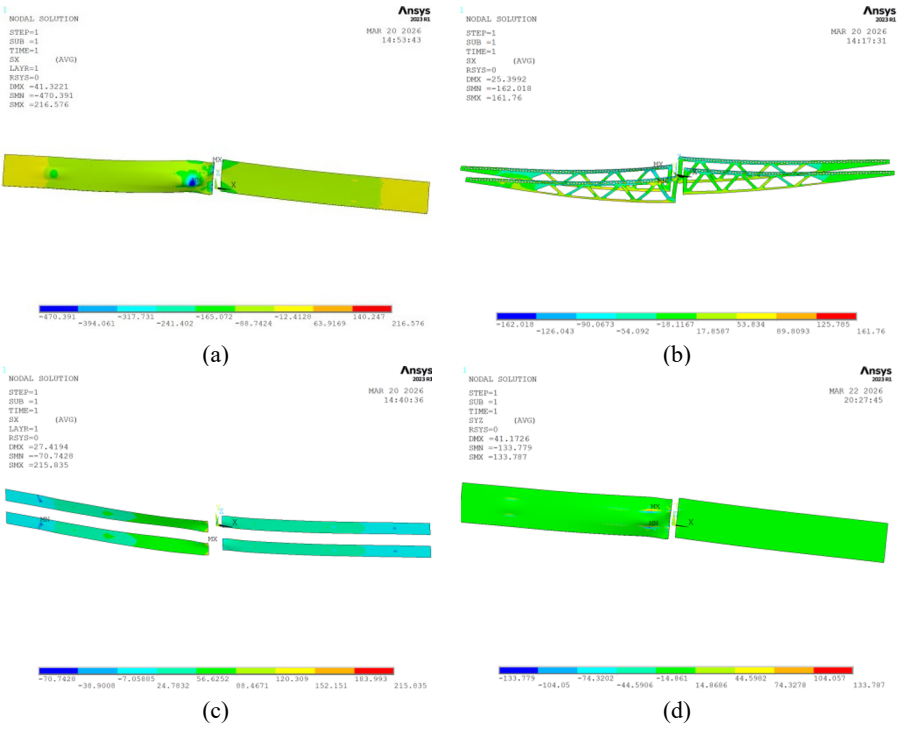



**Fig. 5.** Stress calculation results

### 3.3 Results of the Finite Element Model Stability Analysis

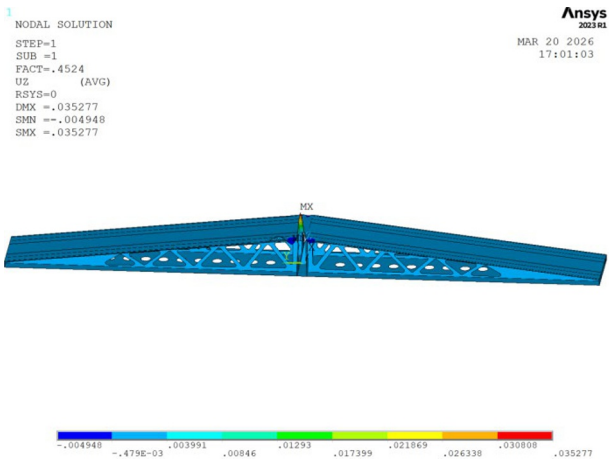



**Fig. 6.** Stability calculation results

Figure 6 shows the buckling modes calculated by the finite element model for Stage 1. The first-order buckling coefficient is 0.353, indicating local buckling of the bridge

deck. For small-span emergency bridges such as the Crater Bridge, the overall stability buckling coefficient is generally required to be greater than 2. As the stability of the bridge deck does not meet the design requirements, the bridge deck must be re-optimised.

# 4 Optimised Design of the Bridge Deck Structure for the Crater Bridge

## 4.1 Introduction to the Optimised Model

Due to their inherent 'ribs', corrugated sandwich structures not only enhance structural stability but also improve shear resistance; therefore, this paper employs a corrugated sandwich structure for the optimised design of the bridge deck, with a triangular sandwich configuration selected. Following an analysis of the calculation results presented earlier, it was found that the bridge deck did not meet the design requirements. Solid elements are well-suited to simulating the shear failure issues occurring in the bridge deck; consequently, solid elements were used to establish a parametric finite element model of the triangular corrugated sandwich structure for the bridge deck of the crater bridge. The other structural members were modelled and analysed using shell elements. The materials and element types used in the model are shown in Figure 7. The solid element mesh type is hexahedral, with a mesh size of 0.5 mm, whilst the shell element mesh type is quadrilateral, with a mesh size of 10 mm. The finite element model is constrained with simply supported ends.

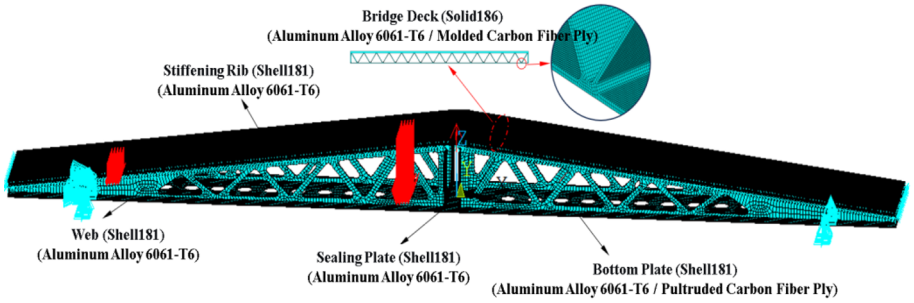



**Fig. 7.** Introduction to the Optimised Model

The structural configuration of the bridge deck is shown in Figure 8. The design variables for the bridge deck are the bridge deck height $H$, Thickness of corrugated sandwich roof panels $t_1$, Thickness of corrugated sandwich floor panels $t_2$, Core thickness $t_3$, Core width $l$, Given that, although structural damage occurred to the crater bridge during the full-load test, it can still be refurbished and reused, the width of the bridge deck will remain as specified in the optimised design from the earlier phase and will not be treated as a design variable.

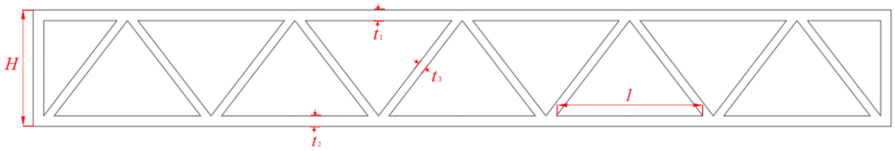



**Fig. 8.** Corrugated sandwich bridge deck

As a temporary emergency structure, the crater bridge is designed to be erected manually in order to minimise the difficulty of its installation; consequently, the optimisation objective for the crater bridge is to achieve the lightest possible weight. The constraints are that the structural strength, stiffness and stability must meet the requirements; the design strength is 200 MPa, and the maximum longitudinal stress in the crater bridge is constrained to 200 MPa. Furthermore, to prevent shear failure of the bridge deck, the ultimate shear strength of 6061-T6 aluminium alloy is 125 MPa, and the maximum shear stress in the bridge deck is constrained to 125 MPa. For box-girder emergency bridges with spans less than 50 m, the allowable deflection is l/120. As the span of the crater bridge is 5 m, the allowable deflection is 5 m/120 = 41.67 mm, and the maximum vertical displacement of the structure is constrained to 41.67 mm. As mentioned earlier, a stability factor greater than 2 is sufficient for small-span emergency bridges; consequently, both the overall stability factor and the local stability factor of the constrained bridge are greater than 2.

## 4.2 Optimisation Results

The final results, rounded using ANSYS commercial software, are shown in Table 2; all dimensions have been rounded to one decimal place. Specifically, the bridge deck height is 35.1 mm, the corrugated sandwich top plate thickness is 5.3 mm, the corrugated sandwich bottom plate thickness is 1.5 mm, the core layer thickness is 1.1 mm, the core layer width is 40.6 mm, and the final weight of a single wheel track on the crater bridge is 176.8 kg.

**Table 2.** Optimisation Results

| | Optimal result |
|---|---|
| Bridge deck height $H$ | 35.1mm |
| Thickness of corrugated sandwich roof panels $t_1$ | 5.3mm |
| Thickness of corrugated sandwich floor panels $t_2$ | 1.5mm |
| Core layer thickness $t_3$ | 1.1mm |
| Core width $l$ | 40.6mm |

The strength, stiffness and stability of the crater bridge are verified below. Figure 9 shows the deflection calculation results for the optimised crater bridge. The maximum vertical displacement of the crater bridge is 17.97 mm, which is significantly less than the permissible deflection of 41.67 mm. There is still a considerable margin in structural stiffness, and the stiffness of the optimised crater bridge meets the design requirements.

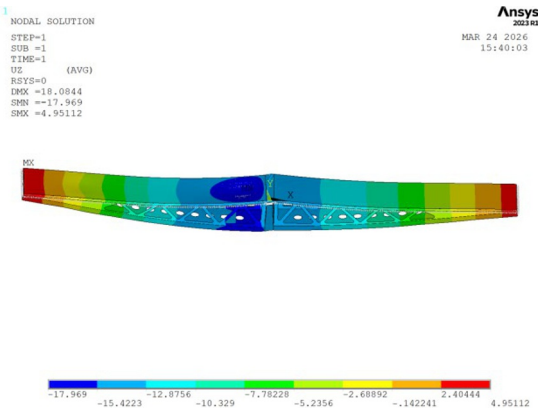



**Fig. 9.** Optimised deflection

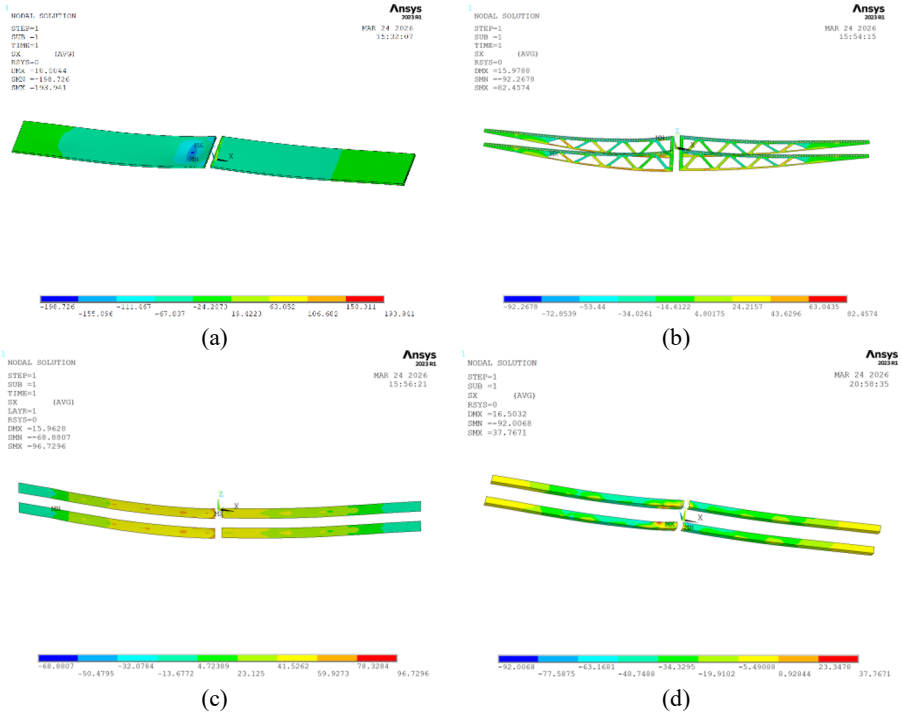



**Fig. 10.** Optimised stress calculation results

Figure 10(a) shows the results of the longitudinal stress analysis for the optimised crater bridge deck. The upper surface of the deck is under compression whilst the lower surface is under tension; the maximum compressive stress is 198.73 MPa and the maximum tensile stress is 193.94 MPa; Figure 10(b) shows the results of the longitudinal stress analysis for the web, with a maximum compressive stress of 92.27 MPa and a maximum tensile stress of 82.46 MPa; Figure 10(c) shows the results of the longitudinal

stress analysis for the bottom plate. The maximum tensile and compressive stresses are both located at the connection ends between the bottom plate and the carbon plate; the maximum compressive stress is 68.88 MPa, and the maximum tensile stress is 96.73 MPa; Figure 10(d) shows the calculated longitudinal stresses in the stiffeners, with a maximum compressive stress of 92.01 MPa and a maximum tensile stress of 37.77 MPa. The longitudinal stresses in the bridge deck, web, bottom plate and stiffeners are all less than 200 MPa, and the strength meets the design requirements.

Figure 11 shows the results of the shear stress analysis for the longitudinal section of the bridge deck. The maximum shear stress in the bridge deck is 110.36 MPa, which is less than the ultimate shear strength of 125 MPa for 6061-T6 aluminium alloy. The maximum shear stress occurs at the junction between the bridge deck and the web, and there is still a certain margin of safety, thus meeting the design strength requirements.

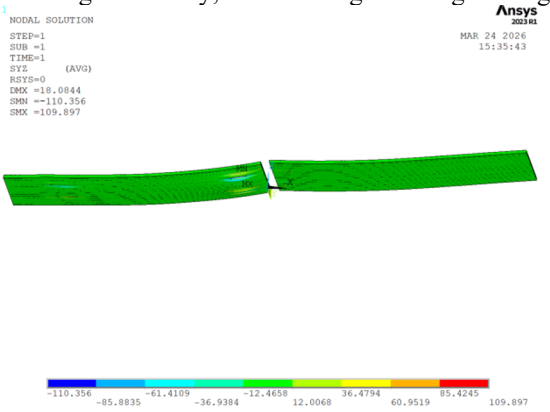
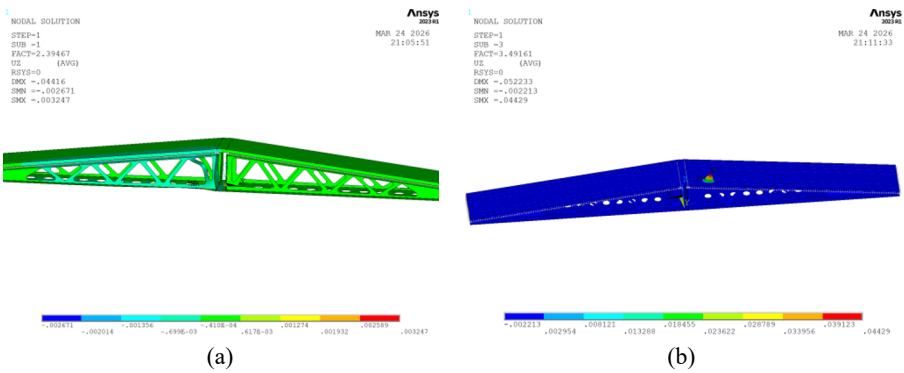



**Fig. 11.** Optimised shear forces in the bridge deck




(a) (b)

**Fig. 12.** Stability calculation results

The first- and second-order buckling coefficients of the optimised finite element model of the Crater Bridge are both approximately 2.39, corresponding to web buckling following the opening at the mid-span, as shown in Figure 12(a). The third-order buckling coefficient is 3.49, corresponding to buckling of the core layer of the corrugated

sandwich deck at the mid-span, as shown in Figure 12(b). The buckling modes for the subsequent stages correspond to buckling of the web at various locations and of the core layer of the bridge deck, respectively; these will not be listed individually here. The bridge deck still has a certain margin of stability and meets the design requirements.

## 5 Conclusions

A parametric finite element model was established for a craters-type bridge deck with a corrugated sandwich structure. Shear stress in the bridge deck was incorporated as a constraint, and optimisation was performed using the zero-order and first-order optimisation algorithms built into the ANSYS commercial software. This ultimately determined the optimal configuration for the craters-type bridge, with the weight of a single wheel track on the bridge set at 176.8 kg, thereby meeting the weight requirement for a single wheel track on the craters-type bridge. The optimised potholed bridge meets the design requirements for strength, stiffness and stability. The web, stiffeners and bottom plate of the potholed bridge still possess a significant margin of strength, indicating that small-span potholed bridges are strength-limited under localised concentrated loads. This provides new insights for the subsequent design of small-span box-girder emergency bridges.

## References

1. Yang L., Kou H. A study on economic impact of natural disasters—A case study of Wenchuan Earthquake[J]. Science Research Management, 2017, 38(6): 51-58.
2. Ding D., Yang S., Song X., et al. Brief analysis on the discussion of property losses in the investigation of common geological disasters in Guizhou Province[J]. West-China Exploration Engineering, 2023, 35(11): 9-11.
3. Brittani R R, Ashley P T. Portable and rapidly deployable bridges: historical perspective and recent technology developments[J]. Journal of Bridge Engineering, 2013, 18: 1074-1085.
4. Yeh F Y, Chang K C, Sung Y C, et al. A novel composite bridge for emergency disaster relief: Concept and verification[J]. Composite Structures, 2015, 127: 199-210.
5. Zeng Z., Zhao Q., Wu Y., et al. Cost-effectiveness analysis of HFRP-aluminum alloy composite truss emergency bridge[J]. Journal of Nanjing Tech University (Natural Science Edition), 2025, 47(1): 73-81.
6. Liu C., Zhang Q., Li F. Vibration characteristics analysis of externally prestressed assembled GFRP emergency bridge with mid-span top support[J]. Journal of Army Engineering University, 2026, 5(2): 42-50.
7. Du B., Liu H., Pan X., et al. Research progress on fusion bonding of thermoplastic composite sandwich structures[J]. Acta Materiae Compositae Sinica, 2022, 39(7): 3044-3058.
8. Xia F K, Yu T X, Durandet Y, et al. Triangular corrugated sandwich panels under longitudinal bending[J]. Thin-Walled Structures, 2021, 169: 108359.
9. Roh H S, Kim J S. Structural optimization of hydrogen storage vessel for type IV composite pressure vessel considering burst pressure[J]. International Journal of Hydrogen Energy, 2023, 48(12): 4891-4906.
10. Prabu B, Kumaran S, Uthayakumar M. Bending strength analysis of hybrid sandwich composite ship hull structures[J]. Ships and Offshore Structures, 2022, 17(8): 1805-1815.

11. Burris D L, Sawyer W G. Wear behavior of PTFE composites: A review[J]. Tribology Letters, 2020, 68(3): 92.
12. Ingrole A, Hao A, Liang R. Energy absorption of 3D printed multi-layer corrugated sandwich panels with negative Poisson's ratio[J]. Composites Part B: Engineering, 2021, 225: 109293.

**Open Access** This chapter is licensed under the terms of the Creative Commons Attribution-NonCommercial 4.0 International License (http://creativecommons.org/licenses/by-nc/4.0/), which permits any noncommercial use, sharing, adaptation, distribution and reproduction in any medium or format, as long as you give appropriate credit to the original author(s) and the source, provide a link to the Creative Commons license and indicate if changes were made.

The images or other third party material in this chapter are included in the chapter's Creative Commons license, unless indicated otherwise in a credit line to the material. If material is not included in the chapter's Creative Commons license and your intended use is not permitted by statutory regulation or exceeds the permitted use, you will need to obtain permission directly from the copyright holder.

